

Isospin-Forbidden and -Allowed $^{16}\text{O}(d,\alpha)^{14}\text{N}$ Reactions*

P. L. Jolivet[†]

Department of Physics, University of Wisconsin, Madison, Wisconsin 53706

(Received 30 March 1973)

Cross sections are reported for the $^{16}\text{O}(d,\alpha)^{14}\text{N}$ transitions to the ground and first excited state for $2 \text{ MeV} \leq E_d \leq 14 \text{ MeV}$ and 8–18 angles. An S -matrix analysis of the isospin-forbidden reaction to the $^{14}\text{N}(2.31\text{-MeV}) T=1$ state yields level parameters, spins, and parities for a large number of ^{18}F intermediate states. Several of these are analogs of $T=1$ levels in ^{18}O . The mechanisms for the isospin-forbidden reaction is entirely compound nuclear and for the isospin-allowed transition is predominantly so. The isospin impurity, averaged over 1–MeV intervals, is 3–10% for $10 \leq E_x(^{18}\text{F}) \leq 20 \text{ MeV}$. Analysis by peak counting indicates that $\Gamma_J/D_J \sim 1$ at $E_x=14 \text{ MeV}$ and that the average coherence width increases from $\sim 100 \text{ keV}$ at $E_x=14 \text{ MeV}$ to $\sim 500 \text{ keV}$ at $E_x=20 \text{ MeV}$.

I. INTRODUCTION

This paper reports differential and total cross sections on the $^{16}\text{O}(d,\alpha)^{14}\text{N}$ ground- and first-excited-state transitions for $2 \leq E_d \leq 14 \text{ MeV}$ and average total cross sections to the second excited state for $7 \leq E_d \leq 14 \text{ MeV}$. The emphasis is on the isospin-forbidden reaction leading to the 2.31-MeV ($T=1$) state in ^{14}N and on an extensive S -matrix analysis which identifies many isospin-mixed states in ^{18}F . The allowed transitions received a much less extensive Legendre polynomial analysis.

Many authors have reported on the $^{16}\text{O}(d,\alpha)^{14}\text{N}$ reaction emphasizing either the allowed or forbidden reactions. The relevant papers are listed in Ajzenberg-Selove¹ supplemented by Jobst.² Despite these extensive data there remained questions concerning the reaction mechanism, the spectroscopy of ^{18}F , and the nature of the ^{18}F states that contribute to the isospin-forbidden reaction.

All workers agree that there is a large compound-nuclear contribution to the (d,α) cross sections in the region studied. However, Cords, Din, and Robson³ claim the allowed reactions also show an appreciable direct contribution at $E_d=6.26 \text{ MeV}$. Jobst,² with more extensive data in the same region, interprets his rapid fluctuations in terms of compound-nuclear states. The isospin-forbidden reactions should show no first-order direct contributions. However, Noble^{4,5} has suggested two semidirect mechanisms which could make some small contributions.

Analysis of the compound-nucleus contribution to the isospin-forbidden cross section may test several assumptions and consequences of the Coulomb mixing mechanism. The present experiment includes the region, $6-10 \leq E_x(^{18}\text{F}) \leq 14-18 \text{ MeV}$, that Wilkinson⁶ suggested for maximum isospin mixing in ^{18}F . In this region levels of the same

spin and parity but different isospin should be dense enough for mixing by the Coulomb force ($\langle H_c \rangle \sim 100 \text{ keV}$),⁶ but still narrow enough that appreciable mixing occurs before decay. The low density of $T=1$ states (inferred from ^{18}O data) limits the lower E_x for appreciable isospin mixing. The upper limit depends upon the width, Γ_J , and spacing, D_J , of levels the same J^π and will thus be spin-dependent.⁷ We note that the limits will also depend upon the fluctuations of $\langle H_c \rangle$, Γ_J , and D_J about their mean values.

An analysis⁸ of some data of Jobst, Messelt, and Richards⁹ indicated that the forbidden (d,α) reaction could be a powerful and selective spectroscopic tool in the very complex region of ^{18}F studied here. Because of the spin and parity combination ($1^+ + 0^+ \rightarrow 0^+ + 0^+$) only natural-parity states can contribute. These same spin and parity properties reduce the S -matrix expansion to manageable proportions.⁸ An enhanced selectivity arises because the state must be both isospin mixed and moderately narrow.

If the isospin mixing is not too large, then isospin is still an approximate quantum number and one can look for correspondences to the other members of the $T=1$ triad, ^{18}O and ^{18}Ne . We do in fact see in ^{18}F many of the analog states. If the mixing is strong, we hoped to see if it arises from mirror configurations as in the famous ^8Be cases or whether the analog state spreads over many neighboring levels.

II. EXPERIMENTAL PROCEDURES

The deuteron beam from an EN tandem Van de Graaff entered the differentially pumped scattering chamber described by Tollefsrud and Jolivet.¹⁰ The gas was research grade O_2 (99.999% pure). No impurities other than ^{18}O (0.2%) were detected. The pressure of 10–25 Torr gave a target thick-

ness of ≤ 6 keV and usually ≤ 2 keV. This thickness varied with angle and energy. The α particles were detected in silicon surface-barrier detectors thin enough to keep deuteron and proton energy losses below those of the α groups of interest. An on-line computer (DDP-124) stored the data and permitted its later reduction to cross section. Peaks were either summed or fitted with a Gaussian line shape using the computer and a light gun-cathode-ray tube (CRT) interface.

Uncertainties are discussed in detail in Ref. 11. Random errors are $\sim 2\%$. Systematic errors are $\leq 1.6\%$ except for a possible beam-heating effect which we estimate may have reduced our reported cross sections by $\sim 2\%$. Runs were long enough to keep the statistical uncertainties for α_1 at the peak of most angular distributions to $\leq 3\%$. Thus the average statistical uncertainty for the forbidden cross section is 4–5%, but it is larger where the cross section is very small. For the allowed groups the statistical error is usually negligible. To avoid troublesome energy shifts between running periods we took data simultaneously at all angles. Deuteron energy steps were 10 keV at the lower energies and increased succes-

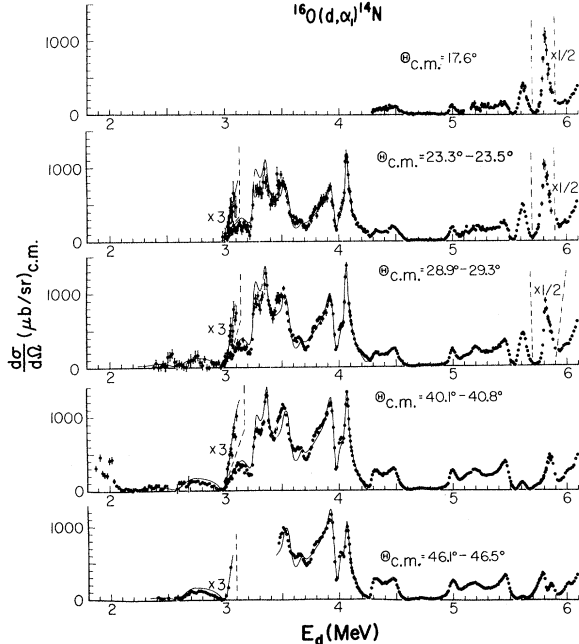


FIG. 1. The isospin-forbidden $^{16}\text{O}(d, \alpha)^{14}\text{N}$ cross sections. Uncertainties (counting statistics and background subtraction only) are shown only when larger than the point size. The data, taken at fixed laboratory angles, correspond to the center-of-mass angles indicated. The solid line for $2.4 \text{ MeV} \leq E_d \leq 4.4 \text{ MeV}$ results from the ^{18}F level parameters of Table III. In other regions lines are only to guide the eye.

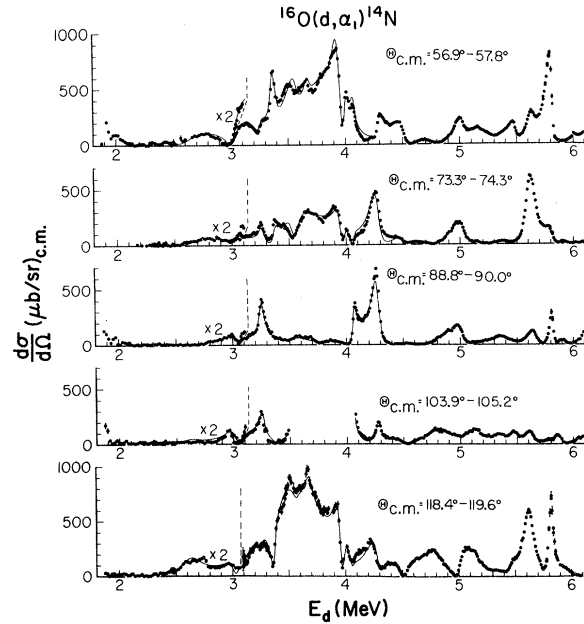


FIG. 2. The same as Fig. 1 but for different angles.

sively to 15, 20, and finally 30 keV above $E_d = 10.5$ MeV. The detector array consisted of 8 detectors at the lowest energies and 18 above $E_d = 10.5$ MeV. The number increased with energy as the angular distributions became more complex.

III. RESULTS

Figures 1–9 display most of the isospin-forbidden α_1 data. Figures 10 and 11 show only a few samples of the data for the ground-state transition.¹¹

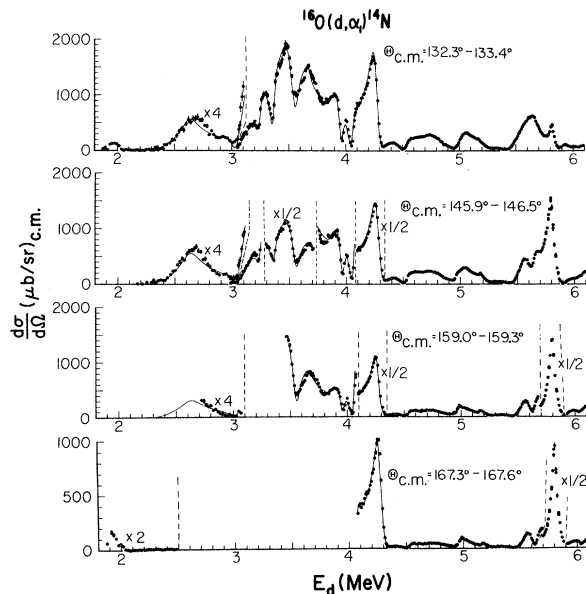


FIG. 3. The same as Fig. 1 but for different angles.

The data taken at fixed laboratory angles correspond to slowly varying center-of-mass angles as indicated in the figures. Figures 12–14 show a few angular distributions for α_0 and α_1 selected from the approximately 800 taken for each final state. The fits are discussed below. The α_0 and α_1 cross sections are also available in tabular form, see Ref. 11.

Where comparisons are possible, our cross sections agree well with Jobst²; Jobst, Messelt, and Richards⁹; Cords, Din, and Robson³; and Dietzsch *et al.*¹²

IV. ANALYSIS

Isospin-Allowed Data

The cross sections for the allowed (d, α_0) and (d, α_2) reactions were expanded in Legendre poly-

nomials. Thus

$$\frac{d\sigma}{d\Omega} = \sum_{\nu=0}^{2L} a_{\nu} P_{\nu}(\cos\theta). \quad (1)$$

The highest-order polynomial needed is limited by the angular momenta involved in the reaction, i.e., L is at most the minimum of the incoming or outgoing orbital angular momentum or the highest spin excited in the compound nucleus. As compound-nuclear states of $J=l$ and $l \pm 1$ (the channel spin is 1) are excited for a given orbital angular momentum, we can set limits on the spins and parities of isolated levels in the allowed reactions by observing the L needed to fit the angular distributions at resonance. Table I shows some of the prominent resonances seen in the (d, α_0) transition and gives spin and parity limits. Figures

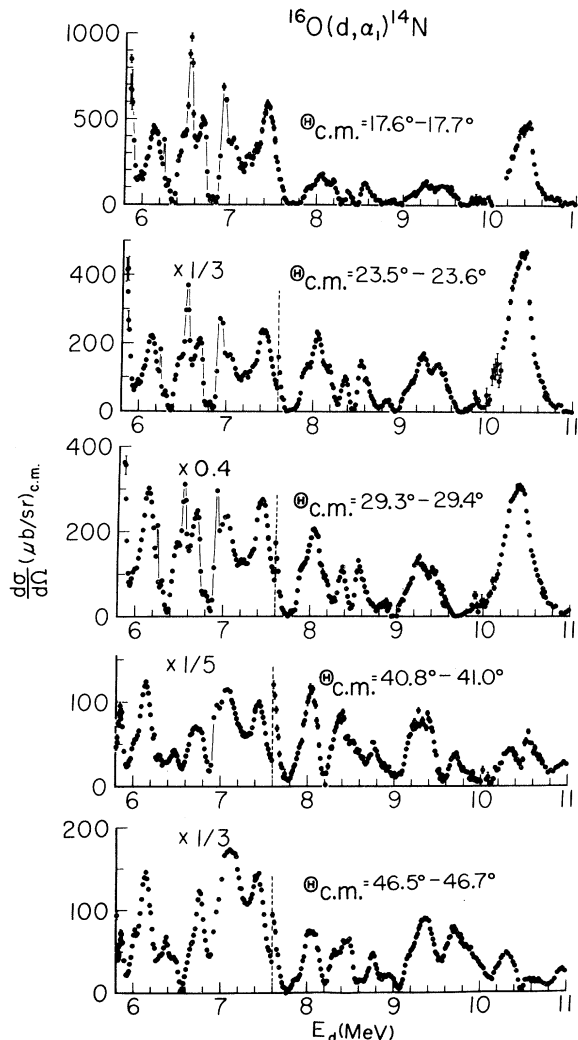


FIG. 4. The same as Fig. 1 but for different energies and angles.

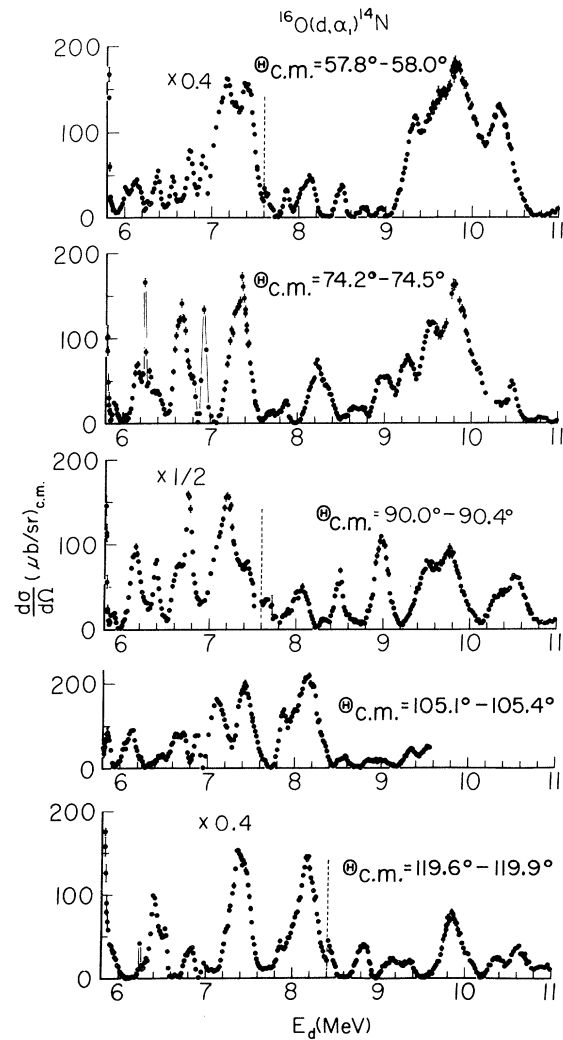


FIG. 5. The same as Fig. 1 but for different energies and angles.

15 and 16 show the coefficients of the Legendre polynomial expansion in the region where these resonances are found, while Fig. 14 shows some sample angular distributions and fits. In Table II the average total cross sections, $\langle\sigma_T\rangle$, for the allowed groups are calculated from the expansion coefficient a_0 , since $\sigma_T = 4\pi a_0$.

Isospin-Forbidden Data

Since the isospin-forbidden channel involves the spin system $0^+ + 1^+ \rightarrow 0^+ + 0^+$, the partial-wave expansion is very simple as we have reported earlier.⁸ Such an expansion is of course independent of reaction mechanism, but the resultant energy dependences of the partial-wave amplitudes show strong resonances and hence imply compound-

nucleus formation. The expansion is

$$\frac{d\sigma}{d\Omega} = \frac{\chi^2}{12} \sum_{l=1}^L \left| \frac{2l+1}{[l(l+1)]^{1/2}} S_l \frac{dP_l(\cos\theta)}{d\theta} \right|^2, \quad (2)$$

where S_l is the complex S matrix element for the l th partial wave and L is the maximum partial wave needed. We note also that $l_i = l_f = J$ and only natural parity states of the compound system can contribute. Furthermore, $l \neq 0$ and all cross sections vanish for $\theta = 0$ and π .

A computer program used Eq. (2) to extract the energy-dependent S matrix elements from the cross sections. Figures 17–19 display a set of the S matrix elements. Because of the squaring in Eq. (2) there are 2^{L-2} sets of S matrix elements with different magnitudes of $|S_l|$ that give identical fits. However, the matrix elements for the highest partial wave, $|S_L|$, are the same for all solution sets; hence any resonances in this partial wave are unambiguously identified. The ambiguity is worst for $l \ll L$, but strong resonances in partial waves other than L often appear in all sets and

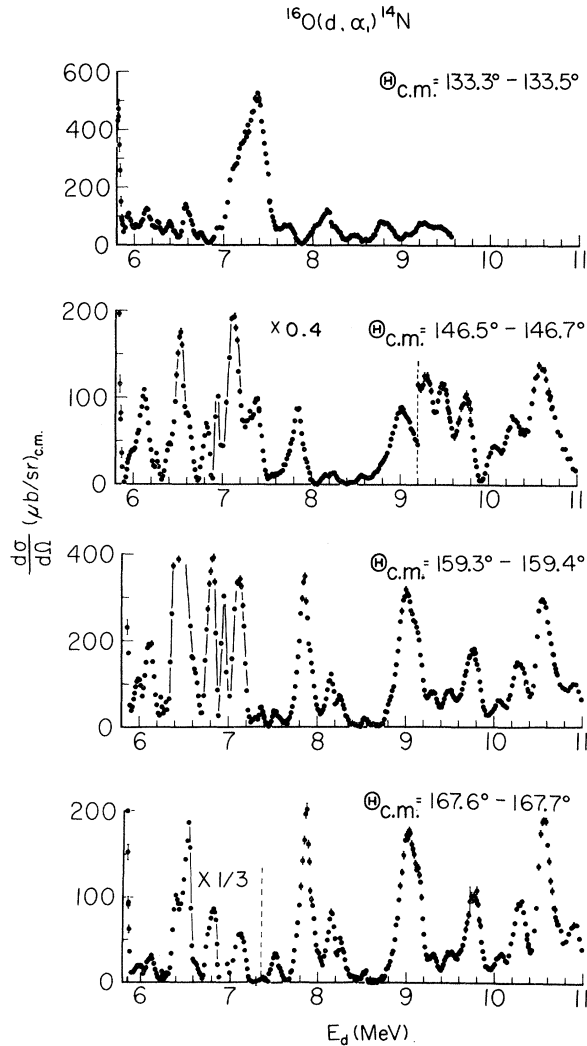


FIG. 6. The same as Fig. 1 but for different energies and angles.

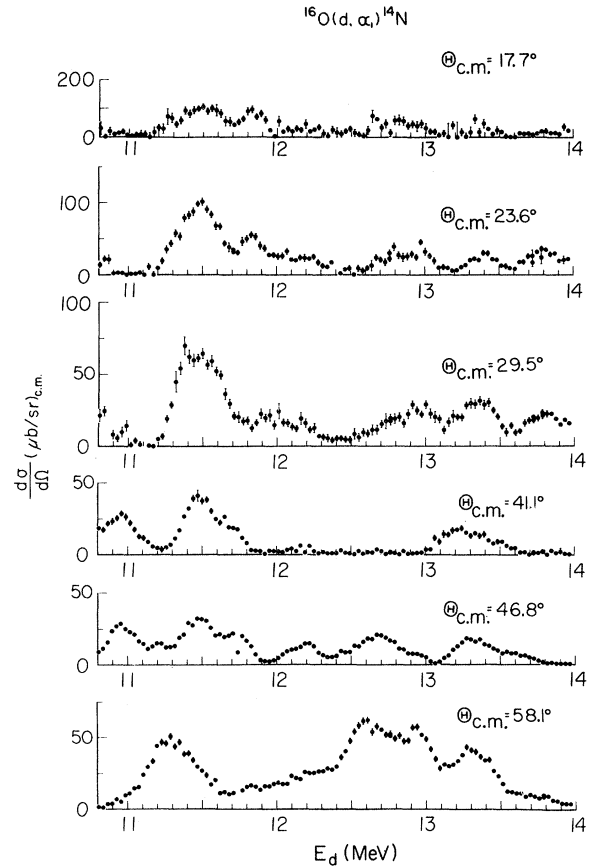


FIG. 7. The same as Fig. 1 but for different energies and angles.

hence are unambiguous. The most difficult problems in the analysis were sorting the degenerate solutions into consistent energy-dependent sets and then selecting the "physical" solution.

Earlier reports^{11,13} outline our procedures.

Briefly, all solution sets were calculated after first sorting the complex roots of the scattering amplitude. The simplest solution set we choose as the "physical" solution (a criterion suggested by a computer experiment¹³). Figure 17 shows the relative complexity of two solutions. In the figure, arrows mark the energies where there is structure in the unambiguous highest partial wave. At these energies the unprimed "physical" solution shows much less structure in the lower partial waves than the primed solution. Thus the unprimed solution will require fewer levels to fit the S matrix elements.

We next try to parametrize the physical solution

set of S_l with a coherent sum of Breit-Wigner resonances:

$$S_l = \sum_{\lambda} \frac{a_{\lambda} + i b_{\lambda}}{E - E_{\lambda} + \frac{1}{2} i \Gamma_{\lambda}}, \quad (3)$$

where E_{λ} and Γ_{λ} are the energy and total width of the state λ with $J^{\pi} = l^{(-)}$. The numerator $a_{\lambda} + i b_{\lambda}$ is identified as $(\Gamma_d \Gamma_{\alpha_1})^{1/2}$ for narrow levels. For wide levels, however, the numerator cannot be associated with a product of partial widths which are independent of the way in which the state is formed as decay occurs before isospin mixing is complete. Thus the measured decay width depends upon the isospin of the entrance channel. This fit in terms of Breit-Wigner resonances is also shown in Figs. 17-19. All $|S_l|$ and cross section data at four angles were fitted simultaneously for $2.8 \leq E_d \leq 4.2$ MeV and the fits to the data are shown in Figs. 1-3. Because of the difficulties in selecting the proper set of S matrix elements and the large number of low spin levels expected, the present

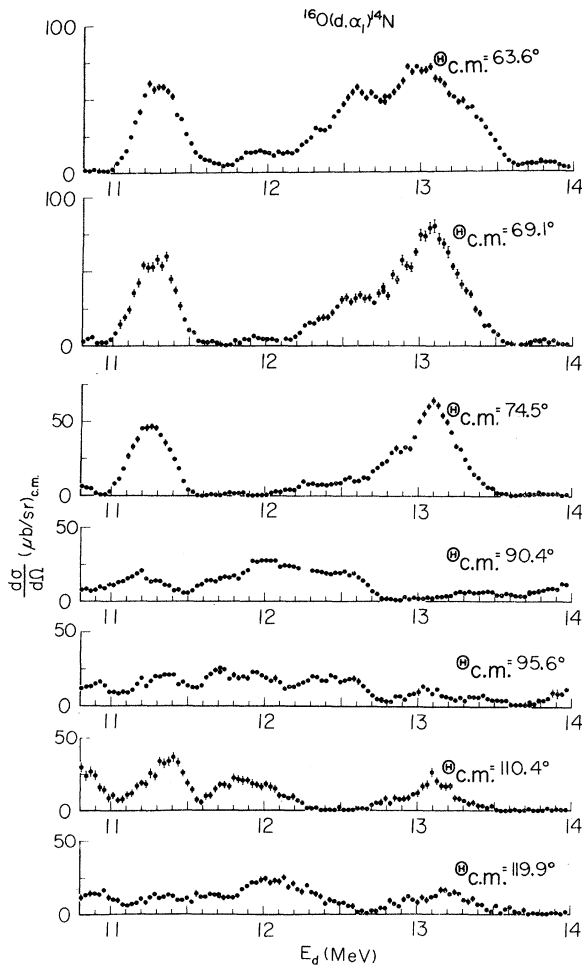


FIG. 8. The same as Fig. 1 but for different energies and angles.

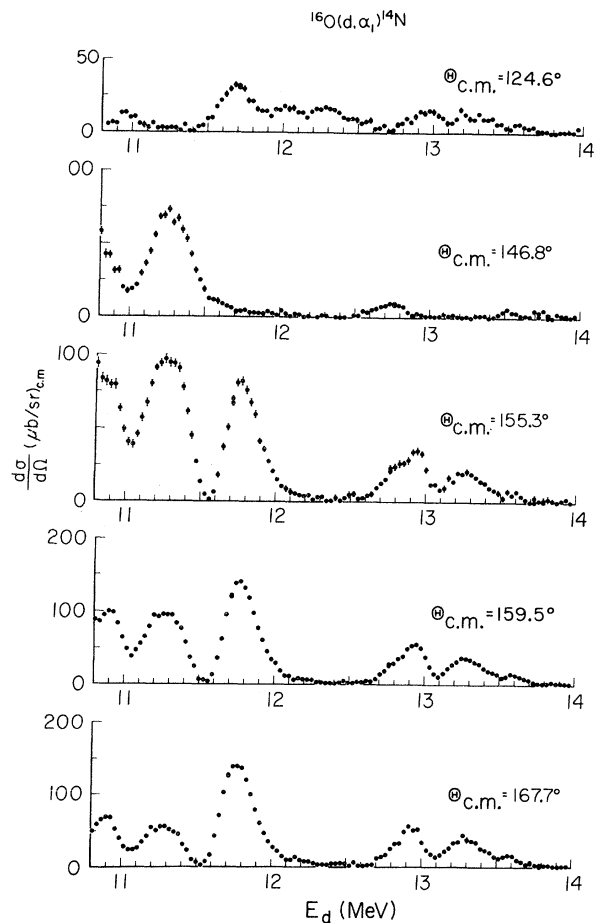


FIG. 9. The same as Fig. 1 but for different energies and angles.

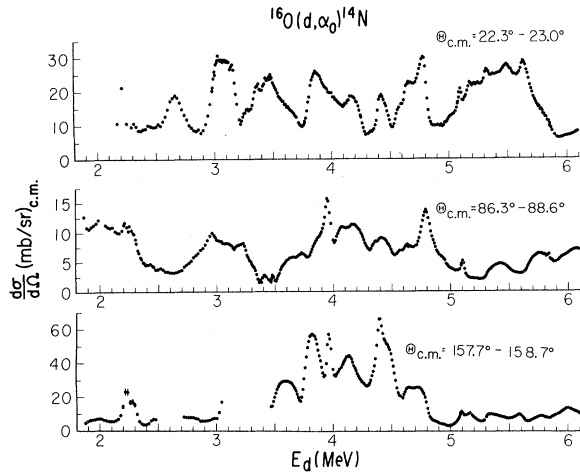


FIG. 10. Similar to Fig. 1 except these are samples of the simultaneously taken isospin-allowed $^{16}\text{O}(d, \alpha)^{14}\text{N}$ cross sections. The complete data are available in tabular form. See Ref. 11.

fits above $E_d = 6$ MeV for the lower partial waves are of marginal significance. Table III shows the levels and parameters used for the fits of Figs. 17–19. The states certainly identified and not subject to alteration from the ambiguities mentioned above are indicated in the footnotes. Uncertainties in the level parameters are difficult to assess, but widths of well-defined levels we estimate are good to $\pm 15\%$. The excitation energy probably has an uncertainty equal to 15% of the level width.

V. REACTION MECHANISM

We find that the compound-nuclear contribution is important at all energies studied, that it prob-

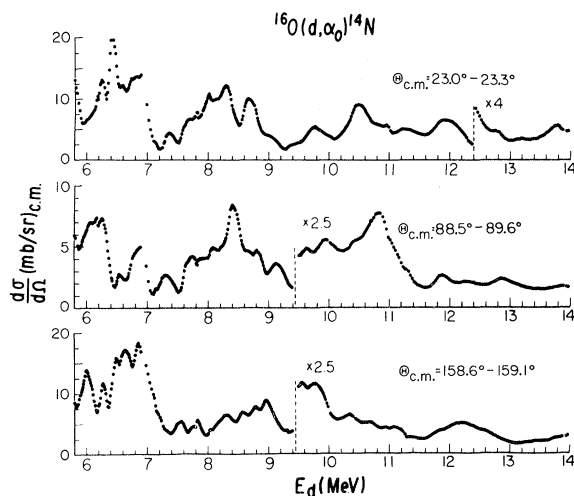


FIG. 11. The same as Fig. 10 but for different energies.

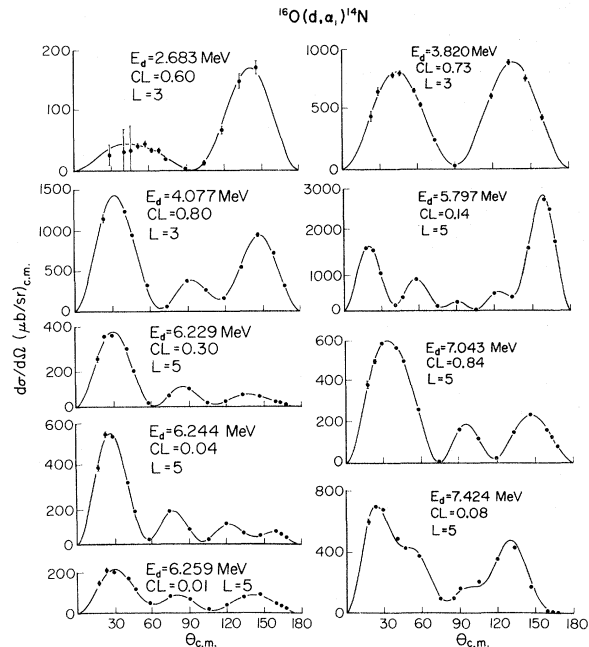


FIG. 12. Sample distributions for the isospin-forbidden reaction. The lines are the fits to the data using Eq. (2). CL is the confidence level and L is the highest partial wave used to fit the data. Uncertainties (statistical) are indicated only when larger than the point size.

ably predominates in the allowed transitions, and that it accounts for all of the forbidden cross section. There is no *a priori* reason for the absence

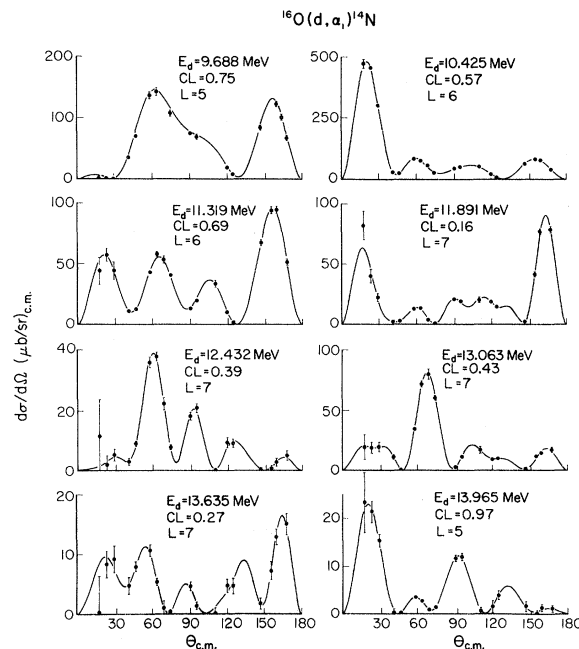


FIG. 13. The same as Fig. 12 but for different energies.

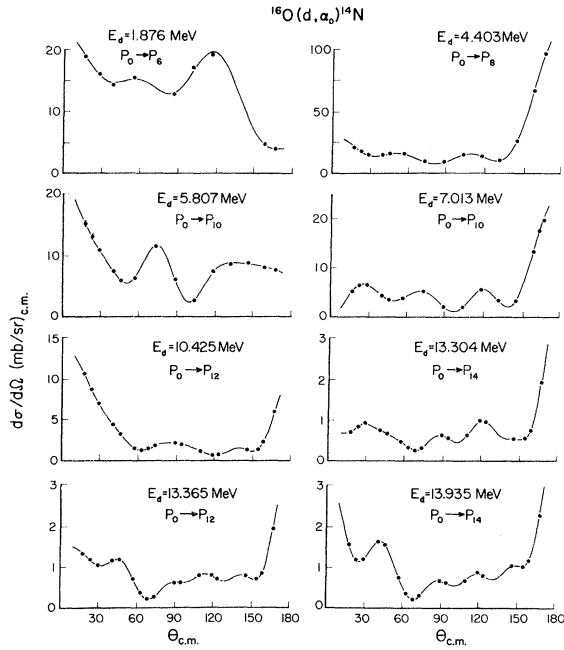


FIG. 14. Samples of the isospin-allowed angular distributions. The lines are Legendre polynomial fits using $P_0 \rightarrow P_n$. Statistical uncertainties are smaller than the points. The series above $E_d = 13$ MeV shows that the forward-angle cross sections are changing rapidly, implying compound-nuclear effects.

of a direct contribution to α_0 and α_2 . However, a one-step direct reaction for α_1 is forbidden by spin and parity restrictions. In addition the common view is that the Coulomb force is too weak to introduce much isospin mixing in the short time

TABLE I. Some $T=0$ states of ^{18}F seen as prominent resonances in the $^{16}\text{O}(d, \alpha_0)^{14}\text{N}$ reaction.

E_d (MeV)	E_x (MeV)	J
1.9	9.2	$3^{\pm}, 4^{-}$
2.22	9.50	$2^{\pm}, 3^{+}$
2.28	9.55	$2^{\pm}, 3^{+}$
3.05	10.24	$3^{\pm}, 4^{-}$
3.12	10.30	≥ 2
3.47	10.61	$4^{\pm}, 5^{+}$
3.80	10.90	≥ 2
3.95	11.04	$3^{\pm}, 4^{-}$
4.38	11.42	$4^{\pm}, 5^{+}$
4.57	11.59	$5^{\pm}, 6^{-}$
4.80	11.79	≥ 3
4.93	11.91	$5^{\pm}, 6^{-}$
5.11	12.07	$4^{\pm}, 5^{+}$
5.6	12.5	≥ 3
6.2	13.0	≥ 4
6.35	13.15	$5^{\pm}, 6^{-}$
7.6	14.3	≥ 4

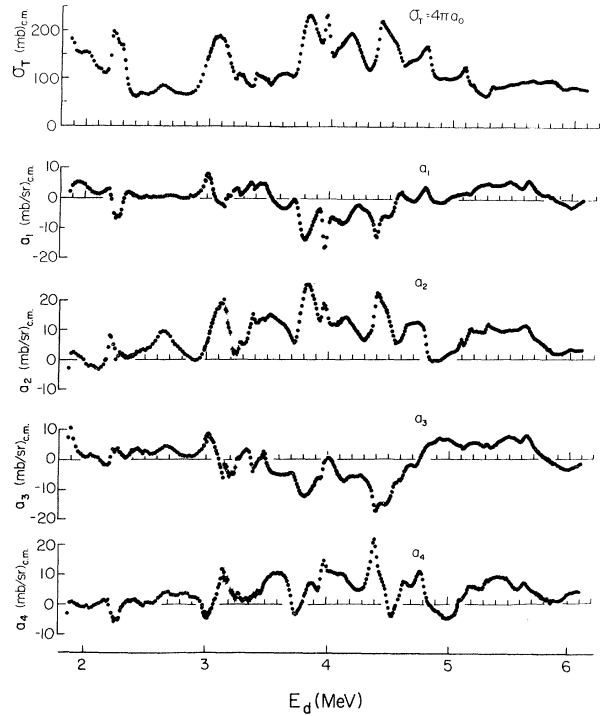


FIG. 15. Coefficients of the Legendre polynomial expansion for the isospin-allowed $^{16}\text{O}(d, \alpha_0)^{14}\text{N}$ transition.

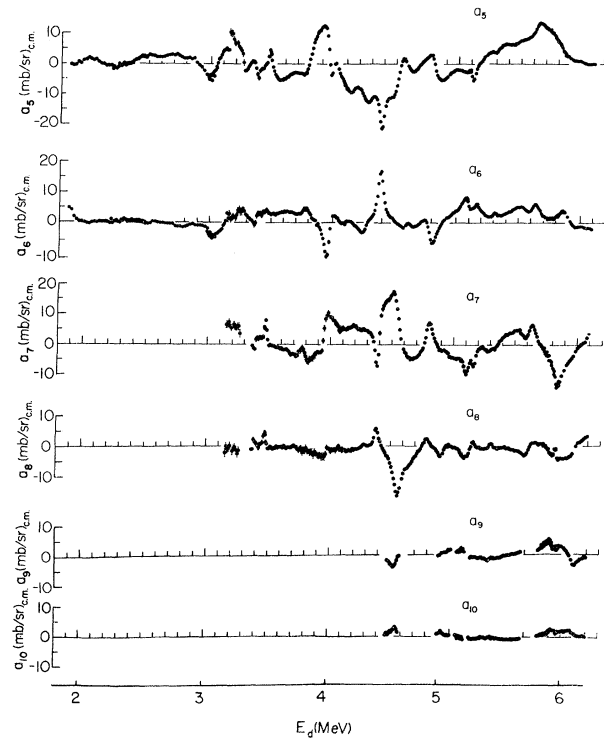


FIG. 16. Same as Fig. 15 but for the high-order coefficients.

span of a direct reaction.

For the allowed groups our conclusions rest on the following evidence. First there are significant fluctuations in the cross sections at all energies (Figs. 10, 11, and 14). Second, Hauser-Feshbach (H-F) calculations presented by Dzubay,¹⁴ for $5 \leq E_d \leq 9$ MeV at $\theta_{\text{c.m.}} \sim 30^\circ$ and $9 \leq E_d \leq 12.5$ MeV at $\theta_{\text{c.m.}} \sim 168^\circ$, are in very good agreement with the magnitude of the cross sections. An extrapolation of his curves agrees well with our cross sections to $E_d = 14$ MeV. Because the level density is only moderately high there are significant fluctuations about the H-F value. Third, the ratio of forbidden to allowed cross section does not decrease substantially as E_d approaches 14 MeV (Table II). Since direct effects are negligible for the forbidden reaction, this constant ratio precludes any significant change in the direct contribution to the allowed reactions. Finally, the total cross sections (Table II) for α_0 and α_2 are nearly equal up to $E_d = 14$ MeV if we allow for the expected fluctuations. This result agrees with H-F predictions but would be surprising for a direct reaction in view of the very different final-state wave functions.

Cords, Din, and Robson³ argue that the excess of the (d, α_0) cross section for $4.25 \leq E_d \leq 8.25$ MeV indicates substantial direct contribution. However, this excess does not continue at higher energies and so represents only a fluctuation. Our Legendre polynomial analysis indicates that high-spin states are not evenly distributed with energy and do contribute significantly to the total cross section in this region.

At somewhat higher energies ($14.5 < E_d < 19.6$ MeV) Yanabu *et al.*¹⁵ report (d, α_0) and (d, α_2) data which they and Honda *et al.*¹⁶ analyze as a sum of knockout and heavy-ion stripping. Yanabu *et al.* claim their data have four characteristics which

TABLE II. Average total cross sections.

E_d (MeV)	E_x (^{18}F) ^a (MeV)	$\bar{\sigma}_T(\alpha_1)$ (mb)	$\bar{\sigma}_T(\alpha_0)$ (mb)	$\frac{\bar{\sigma}_T(\alpha_1)}{\bar{\sigma}_T(\alpha_0)}$	$\bar{\sigma}_T(\alpha_2)$ (mb)	$\frac{\bar{\sigma}_T(\alpha_1)}{\bar{\sigma}_T(\alpha_2)}$
2. → 3.	9.749	0.277	100	0.0028		
3. → 4.	10.638	5.18	141	0.0368		
4. → 5.	11.527	2.26	151	0.0150		
5. → 6.	12.416	1.98	89.1	0.0222		
6. → 7.	13.305	1.53	80.6	0.0189		
7. → 8.	14.194	1.75	41.5	0.0422	43.0 ^b	0.0407
8. → 9.	15.083	0.591	49.2	0.0120	38.4	0.0154
9. → 10.	15.987	0.814	26.8	0.0304	35.2 ^b	0.0231
10. → 11.	16.860	0.563	27.0	0.0209	27.9 ^b	0.0202
11. → 12.	17.749	0.285	18.4	0.0155	19.5	0.0146
12. → 13.	18.637	0.174	13.6	0.0128	13.3	0.0131
13. → 14.	19.527	0.135	9.21	0.0146	10.9	0.0124

^a Calculated at the center of the interval for E_d .

^b The α_2 data for $7 \leq E_d \leq 7.2$ MeV and for $9.8 \leq E_d \leq 10.2$ MeV are missing.

support a direct-interaction interpretation: (1) The total cross section is greater than expected from the compound-nuclear concept; (2) there are both forward and backward angle peaks at almost all energies; (3) the branching ratios for several high-energy α groups are about the same for all energies; and (4) there are resonant-like broad peaks and dips at some energies. Yanabu *et al.* do not document (1) with any calculations. Since their data join smoothly to ours at lower energy and our cross sections are consistent with H-F estimates, we are skeptical of (1). Most of the other cited characteristics seem to us consistent with the compound-nuclear mechanism being dominant. However as E_d increases toward 20 MeV,

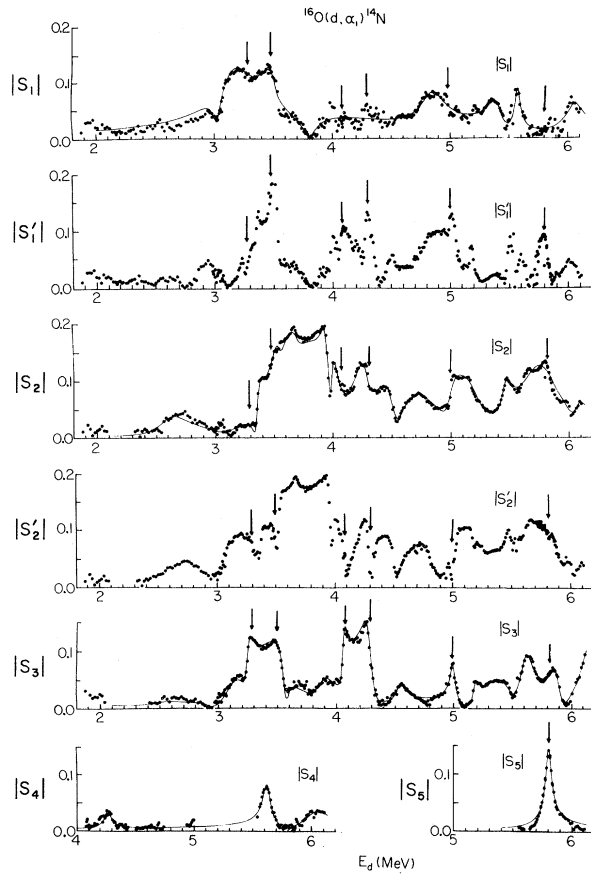


FIG. 17. S matrix elements found by fitting the $^{16}\text{O}(d, \alpha)^{14}\text{N}$ data with Eq. (2). Uncertainties are $\sim 5\%$ for the highest partial wave at each energy and are progressively larger for the lower partial waves. The lines are the fit to the S matrix elements using the level parameters of Table III. Below $E_d = 5.5$ MeV only three partial waves are usually needed. The “unphysical,” primed, and the “physical,” unprimed, solutions are both shown. Arrows mark energies where strong structure in $l = 3$ greatly influences the “unphysical” solutions while the “physical” solution is relatively smooth.

their data do show a net forward-peak asymmetry which, if not a fluctuation, may indicate that direct contributions become appreciable in the upper portion of their energy range.

In conclusion, strong compound-nucleus effects are present for $E_d < 20$ MeV. Direct effects are probably small for $E_d < 14$ MeV and reliable quantitative estimates have not yet been made.

As indicated earlier, we do not expect sizable direct contributions to α_1 . The α_1 cross section also has the rapidly fluctuating character of a compound-nuclear reaction. These α_1 fluctuations are more marked than for the allowed groups because only one independent cross section¹⁷ occurs instead of the possible five for α_0 and α_2 . We find from our S-matrix analysis that the high partial waves (which are the most reliable ones) are well fitted at all energies by a few Breit-Wigner resonances. At low energies where we reproduce the cross sections we see that only sums of Breit-Wigner resonances are necessary. While no slowly varying background is needed, we cannot exclude a small direct contribution.

If a direct component exists and is forward peaked, it must be very small in the forbidden

data. Above $E_d = 12$ MeV the integrated cross section in the forward hemisphere is generally larger than that from 90 to 180° . However, the strength is concentrated near 60° in the second lobe of the angular distribution rather than at the more forward angles associated with a stripping peak (Fig. 13). At the point where the total cross section is smallest ($E_d = 13.605$ MeV) the largest cross section is at extreme backward angles. Even above $E_d = 14$ MeV the data of Jänecke *et al.*¹⁸ demonstrate that compound-nuclear effects are important. Resonances at $E_d = 14.4$ and 15.1 MeV dominate their $\theta_{c.m.} = 20^\circ$ excitation function. In the region $15.5 \leq E_d \leq 18.1$ MeV where Jänecke *et al.* report the cross section as flat within their uncertainties, the tails of the lower-energy resonances must be still important. Their partial angular distribution at $E_d = 15.8$ MeV shows this clearly since the first peak is at the rather large angle $\theta_{c.m.} \approx 20-25^\circ$ where the $l=4$ and 5 partial waves are maximum, whereas at lower energies the first peak is at a smaller angle. A direct reaction occurring at the surface will at these energies involve partial waves up to $l \geq 7$ which has its first peak forward of $\theta_{c.m.} = 15^\circ$. For our data a forward-peaked direct contribution

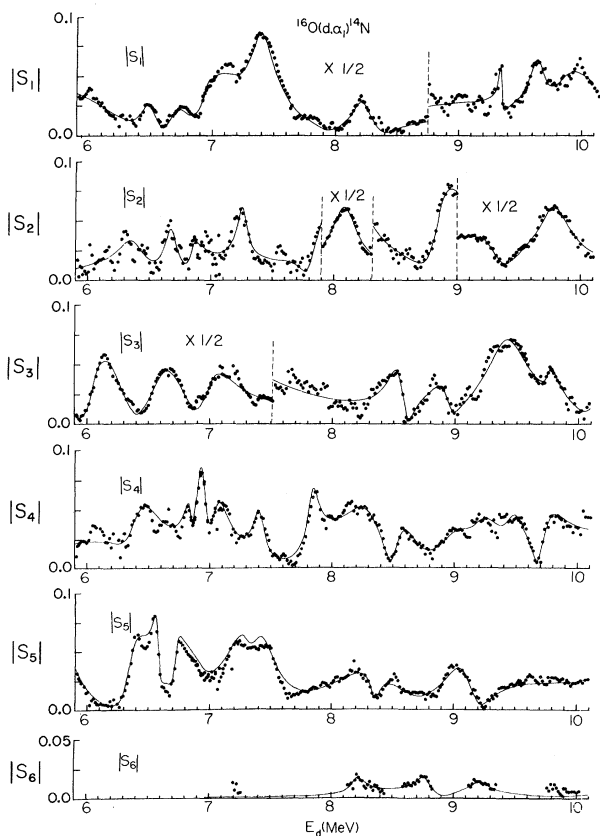


FIG. 18. The same as Fig. 17 for different energies.

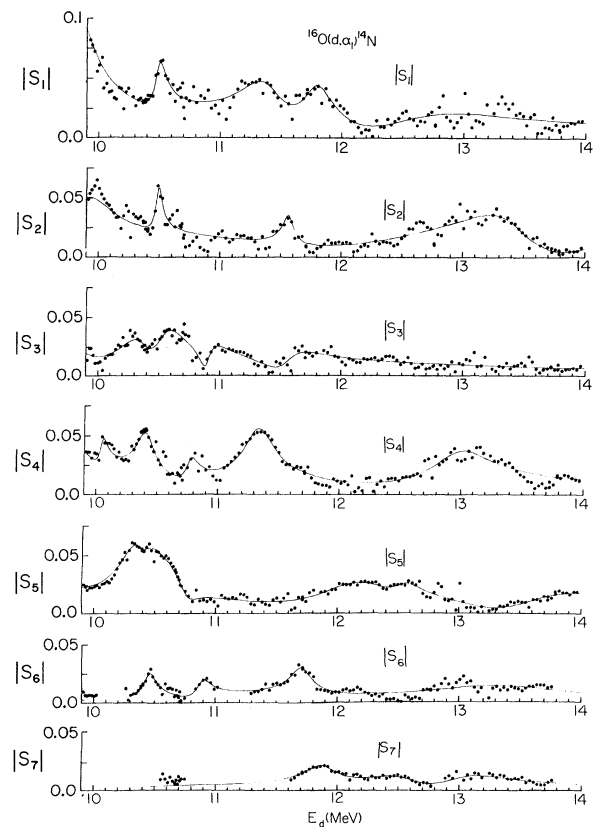


FIG. 19. The same as Fig. 17 for different energies.

TABLE III. Isospin-mixed levels in ^{16}F arranged by J^π . Parameters are those used to fit the S matrix elements [see Eq. (3)].

	E_x (^{16}F) (MeV)	E_d (MeV)	$\Gamma_{\text{c.m.}}$ (keV)	a	b	Strength $ S(E_x) $	Footnotes
$J=1$							
1	10.210	3.021	93	0.0063	0.0029	0.132	
2	10.350	3.179	269	-0.0105	-0.0178	0.136	a
3	10.594	3.454	157	0.0030	-0.0037	0.054	a
4	10.628	3.492	58	0.0011	0.0004	0.036	
5	10.910	3.809	241	-0.0066	0.0029	0.053	a
6	11.107	4.031	1009	0.0121	-0.0107	0.028	b
7	11.831	4.847	179	-0.0102	0.0038	0.108	a
8	12.313	5.390	100	0.0040	0.0018	0.078	cd
9	12.474	5.571	35	-0.0007	-0.0018	0.098	cd
10	13.168	6.353	184	-0.0003	-0.0039	0.038	cd
11	13.443	6.662	77	-0.0017	0.0013	0.049	cd
12	13.607	6.847	88	-0.0008	0.0008	0.023	cd
13	13.959	7.244	69	-0.0008	-0.0016	0.046	cd
14	14.481	7.832	203	0.0015	0.0038	0.036	cd
15	14.703	8.082	169	-0.0006	-0.0115	0.121	cd
16	15.398	8.865	157	-0.0044	-0.0023	0.056	cd
17	15.744	9.255	249	0.0067	0.0040	0.056	cd
18	16.132	9.692	355	0.0078	-0.0039	0.044	cd
19	16.211	9.781	181	0.0081	-0.0027	0.084	cd
20	16.849	10.499	78	0.0016	-0.0003	0.037	cd
21	17.619	11.367	313	0.0024	0.0051	0.032	cd
22	18.002	11.799	203	0.0019	0.0033	0.033	cd
23	18.786	12.682	1072	0.0104	-0.0006	0.017	cd
$J=2$							
1	9.321	2.020	40	0.0	0.0	0.0	ef
2	9.854	2.620	195	0.0033	0.0023	0.037	a
3	10.314	3.138	572	0.0016	-0.0108	0.034	
4	10.516	3.366	46	0.0011	-0.0025	0.105	a
5	10.609	3.471	151	0.0038	-0.0036	0.062	a
6	10.677	3.547	62	-0.0012	-0.0008	0.041	
7	10.704	3.578	375	-0.0048	0.0352	0.168	g
8	10.799	3.684	85	-0.0010	-0.0013	0.034	
9	10.945	3.849	402	-0.0059	-0.0124	0.061	g
10	10.994	3.904	222	0.0025	-0.0072	0.061	g
11	11.029	3.944	78	-0.0011	-0.0078	0.179	
12	11.069	3.989	51	-0.0036	0.0023	0.149	
13	11.304	4.253	475	-0.0235	0.0007	0.088	
14	11.316	4.267	94	0.0025	-0.0036	0.083	
15	11.505	4.480	126	0.0054	0.0002	0.076	
16	11.661	4.655	240	-0.0029	-0.0071	0.057	
17	11.967	5.000	124	-0.0036	-0.0037	0.074	
18	12.136	5.190	219	0.0006	0.0107	0.087	
19	12.359	5.441	78	0.0051	-0.0030	0.135	
20	12.377	5.462	116	-0.0140	0.0103	0.266	
21	12.626	5.742	231	0.0112	0.0023	0.088	cd
22	12.665	5.786	288	0.0106	0.0100	0.090	cd
23	12.814	5.954	441	0.0278	-0.0032	0.113	cd
24	12.989	6.151	648	0.0135	-0.0155	0.056	cd
25	13.287	6.487	99	0.0006	-0.0043	0.078	cd
26	13.499	6.726	146	0.0052	-0.0036	0.077	cd

TABLE III (Continued)

	E_x (^{18}F) (MeV)	E_d (MeV)	$\Gamma_{c.m.}$ (keV)	a	b	Strength $ S(E_x) $	Footnotes
27	13.702	6.954	78	-0.0016	0.0014	0.048	cd
28	13.808	7.074	263	-0.0034	-0.0140	0.097	cd
29	14.098	7.400	166	0.0149	-0.0043	0.166	cd
30	14.833	8.228	124	0.0048	-0.0004	0.069	cd
31	14.906	8.310	1201	-0.0206	-0.0311	0.055	cd
32	15.828	9.349	20	0.0004	0.0002	0.040	cd
33	16.089	9.643	103	0.0021	-0.0006	0.038	cd
34	16.325	9.909	292	0.0046	-0.0024	0.032	cd
35	16.844	10.494	47	0.0010	0.0	0.038	cd
36	17.796	11.567	78	0.0009	0.0006	0.025	cd
37	19.025	12.951	1894	0.0043	-0.0245	0.023	cd
38	19.393	13.366	483	-0.0017	0.0104	0.039	cd
$J=3$							
1	9.259	1.950	30	0.0	0.0	0.0	aef
2	9.701	2.448	372	-0.0026	0.0029	0.019	
3	10.303	3.126	179	-0.0045	0.0047	0.065	a
4	10.417	3.254	48	a -0.0018	0.0016	0.089	a
5	10.642	3.508	236	0.0156	-0.0101	0.140	a
6	10.690	3.562	75	-0.0037	0.0036	0.122	a
7	10.983	3.892	119	0.0002	-0.0013	0.020	a
8	11.140	4.069	35	-0.0002	-0.0020	0.102	af
9	11.264	4.208	238	0.0117	-0.0008	0.088	a
10	11.324	4.276	65	-0.0060	0.0035	0.190	af
11	11.561	4.543	67	0.0008	-0.0009	0.032	a
12	11.961	4.993	32	0.0011	0.0007	0.072	a
13	12.122	5.175	36	-0.0002	-0.0007	0.036	a
14	12.335	5.414	187	0.0036	0.0027	0.043	a
15	12.505	5.606	88	0.0039	-0.0012	0.082	ah
16	12.737	5.867	63	-0.0005	0.0019	0.055	ah
17	12.898	6.048	120	-0.0035	-0.0034	0.072	acd
18	13.031	6.198	248	0.0085	0.0148	0.122	cd
19	13.432	6.650	233	0.0128	0.0059	0.107	cd
20	13.765	7.025	206	0.0099	-0.0008	0.086	cd
21	15.101	8.530	115	-0.0029	-0.0032	0.067	cd
22	15.177	8.616	299	0.0012	0.0074	0.045	cd
23	15.435	8.906	123	0.0018	-0.0014	0.033	cd
24	15.876	9.403	272	0.0110	-0.0061	0.082	cd
25	16.202	9.771	77	0.0009	0.0004	0.023	cd
26	16.701	10.333	296	0.0048	0.0031	0.034	cd
27	16.879	10.533	251	0.0047	-0.0036	0.042	cd
28	17.214	10.911	112	0.0004	-0.0014	0.023	cd
29	17.819	11.592	273	0.0016	-0.0019	0.016	cd
$J=4$							
1	11.314	4.264	38	-0.0003	-0.0008	0.040	af
2	12.515	5.617	47	-0.0016	0.0015	0.083	afh
3	13.064	6.235	10	0.0	0.0	0.0	ae
4	13.204	6.393	254	-0.0182	0.0157	0.168	
5	13.264	6.461	359	0.0234	-0.0117	0.129	
6	13.600	6.839	41	0.0006	0.0002	0.027	
7	13.686	6.936	61	0.0025	-0.0005	0.074	h
8	13.802	7.067	132	0.0027	-0.0020	0.045	h
9	14.103	7.406	73	0.0013	0.0007	0.036	
10	14.487	7.839	76	0.0011	-0.0019	0.051	
11	14.904	8.308	304	0.0044	0.0088	0.057	
12	15.136	8.570	156	0.0032	-0.0013	0.039	
13	15.546	9.032	319	0.0051	0.0015	0.030	cd
14	15.715	9.223	237	0.0041	-0.0008	0.031	cd

TABLE III (Continued)

	E_x (^{18}F) (MeV)	E_d (MeV)	$\Gamma_{\text{c.m.}}$ (keV)	a	b	Strength $ S(E_x) $	Footnotes
15	15.941	9.476	153	0.0024	0.0009	0.030	cd
16	16.182	9.748	149	0.0026	-0.0029	0.046	cd
17	16.449	10.049	52	0.0006	-0.0002	0.022	cd
18	16.766	10.406	135	0.0015	0.0022	0.035	cd
19	17.095	10.777	86	0.0008	0.0001	0.017	cd
20	17.588	11.332	208	0.0030	0.0044	0.045	ac
21	19.059	12.990	416	0.0040	0.0059	0.030	cd
$J=5$							
1	12.664	5.785	379	0.0011	0.0055	0.026	a
2	12.676	5.799	46	0.0003	-0.0039	0.151	afh
3	13.195	6.383	94	-0.0022	-0.0018	0.054	ah
4	13.353	6.561	33	0.0010	0.0003	0.056	afh
5	13.495	6.721	75	-0.0010	-0.0009	0.032	a
6	13.633	6.877	313	0.0021	0.0046	0.029	a
7	13.997	7.286	177	0.0026	0.0028	0.038	ah
8	14.101	7.404	250	0.0064	-0.0001	0.045	ah
9	14.941	8.350	126	-0.0023	-0.0002	0.033	a
10	14.972	8.385	491	0.0089	0.0082	0.044	a
11	15.583	9.073	174	0.0012	0.0039	0.042	a
12	15.810	9.329	1044	0.0159	-0.0126	0.035	ab
13	16.723	10.357	212	0.0058	0.0049	0.064	a
14	16.788	10.431	209	0.0033	-0.0051	0.052	a
15	17.052	10.728	180	-0.0019	-0.0004	0.019	
16	18.300	12.135	554	0.0068	0.0011	0.022	a
17	18.674	12.556	208	0.0012	0.0005	0.011	a
$J=6$							
1	14.822	8.216	91	0.0009	0.0006	0.021	a
2	15.310	8.766	100	0.0001	-0.0010	0.018	a
3	15.696	9.200	174	0.0002	-0.0014	0.014	a
4	16.811	10.457	86	0.0011	0.0002	0.023	a
5	17.194	10.888	88	0.0007	0.0003	0.015	a
6	17.918	11.704	155	-0.0019	0.0010	0.025	a
7	19.341	13.307	911	-0.0055	-0.0039	0.013	b
$J=7$							
1	18.064	11.869	223	0.0009	-0.0019	0.017	a
2	18.620	12.495	395	0.0021	0.0002	0.009	a
3	19.139	13.080	477	0.0023	-0.0022	0.012	a

^a This level is unambiguous in the S matrix elements and the uncertainties in E_x and Γ are estimated to be $\sim 15\%$ of Γ .

^b May be several narrower levels.

^c Possibly an Ericson fluctuation.

^d Uncertain because of ambiguities in the S -matrix analysis.

^e This level was not used in fitting the S matrix elements.

^f An ^{18}O state of same J^π , has been identified near the corresponding E_x (^{18}O).

^g Main components of the 2^+ structure near $E_d = 3.7$ MeV. The structure may possibly be reproduced by another set of levels.

^h A level of the same J^π , approximate width, and E_x (^{18}F) occurs in $^{14}\text{N}(\alpha, \alpha_1)^{14}\text{N}$.

is probably less than $5 \mu\text{b}/\text{sr}$. Such a value is consistent with the upper limits calculated for various direct mechanisms,¹⁹ Coulomb excitation of incoming²⁰ and outgoing particles,²¹ preferential spin-flip,⁴ or the impurities in the reaction particles themselves.²² Evidence for the semidirect

mechanism of Noble⁵(which envisions isospin mixing in one cluster of the compound nucleus followed by a stripping reaction and which results in a large forward-peaked resonant cross section) we find lacking in our data.

Isospin mixing by Coulomb forces in the com-

pound nucleus will yield for an isospin-forbidden reaction different results for three regions of excitation.⁶ At low energies levels are well separated and $\langle H_c \rangle \ll D_J$ for levels of the same spin and parity. Consequently, states have nearly pure isospin and the (d, α_1) cross section will be small. At higher energies the yield may be substantial because $\langle H_c \rangle \sim D_J$ and the states will have large admixtures of different isospin. As the energy further increases the states become thoroughly mixed as $\langle H_c \rangle > D_J$. However, in the incident channel the initial superposition of states will have pure isospin. Other isospin states then mix into the superposition with a time constant $\propto \langle H_c \rangle$. If $\Gamma_J \gg \langle H_c \rangle$, the states will decay before appreciable mixing takes place.

This mechanism suffices for our forbidden cross sections. They are very low below $E_x(^{18}\text{F}) \sim 10$ MeV, ($E_d \sim 3$ MeV), but do show small resonances where $T=1$ states are expected. There is an abrupt increase in these cross sections above $E_d = 3$ MeV. This result should imply a sudden increase in the density of natural parity $T=1$ states in ^{18}F that mix with the abundant $T=0$ states. Indeed, the $^{14}\text{C}(\alpha, \alpha)^{14}\text{C}$ cross section²³ shows a sudden increase at the corresponding excitation in ^{18}O . Our ratio of forbidden to allowed cross sections averages about 2% for $3 \leq E_d \leq 14$ MeV (see Table II). Fluctuations about this value result almost equally from effects in the allowed and forbidden channels.

Although our data go to $E_x(^{18}\text{F}) \sim 20$ MeV (which is 2 to 6 MeV above the energy where Wilkinson⁶ estimated the dynamic criterion would be valid), we find no evidence that isospin conservation reasserts itself. The width of reliably identified levels above $E_d = 12$ MeV [$E_x(^{18}\text{F}) \sim 18$ MeV)] is 200 to 500 keV which is about the average coherence width found for allowed groups. No estimates of the effective isospin mixing are available for this intermediate region where $\Gamma \sim \langle H_c \rangle$. However, for $\langle H_c \rangle \sim 100$ keV the values of $|S_l| \sim 0.02$ (Fig. 19) do not appear unreasonable. In addition, larger $\langle H_c \rangle$ have been suggested in ^9Be (see Barker²⁴) and perhaps ^{12}C (see Braithwaite, Bussoletti, and Cecil²⁵).

Data of Janeke *et al.*¹⁸ indicate that the (d, α_1) cross section remains appreciable to $E_d \sim 15$ MeV ($E_x = 20.8$) and then becomes quite small: $< 10 \mu\text{b}/\text{sr}$ at $\theta_{c.m.} = 20^\circ$. Chesterfield and Parker²⁶ extended the $^{14}\text{N}(\alpha, \alpha_1)^{14}\text{N}$ data to $E_x(^{18}\text{F}) \sim 24$ MeV but found no marked diminution in the yield. Preliminary indications²⁷ are that $^{12}\text{C}(^6\text{Li}, \alpha_1)^{14}\text{N}$ also has a measurable compound-nucleus cross section above $E_x(^{18}\text{F}) = 20$ MeV, i.e., $\sigma(2.31)/\sigma(\text{g.s.}) \sim 1-2\%$. Since $\langle \Gamma \rangle$ increases slowly with energy and one expects fluctuations about $\langle \Gamma \rangle$ and $\langle H_c \rangle$, the small (d, α_1) cross section of Ref. 18 appears anomalous.

If this (d, α_1) cross section indeed remains very small [the data of Ref. 18 are very limited above $E_d = 16$ MeV ($E_x = 21.7$ MeV)], the explanation involves the deuteron channel and not the reassertion of isospin conservation. Perhaps at higher energies much deuteron flux diverts to direct reactions, e.g. to the (d, p) and (d, n) channels.

Lane and Thomas⁷ point out that isospin conservation should reappear in the low partial waves before restoration in the high partial waves, since high-spin states are narrower than low-spin states. Examination of the S matrix elements for the higher energies, Fig. 19, does not confirm this expectation, since the magnitudes are about the same for all partial waves. However, the contribution to the total cross section is weighted by $(2l+1)$ so the high-spin states do dominate the cross section. Thus the uncertainties in the $|S_l|$ values for low l are large. Also the ambiguities in the analysis are largest for the low partial waves. Nonetheless, there remains a detectable contribution from the low partial waves. Several explanations are possible. First, the contributions from moderately wide levels, $\Gamma \lesssim 10\langle H_c \rangle$, may be important and/or perhaps the low-spin levels may be only slightly wider than those of high spin.²⁸

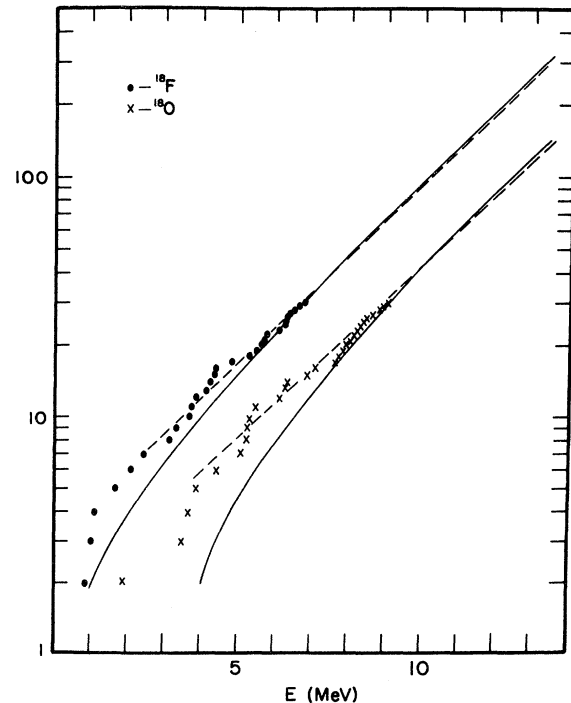


FIG. 20. Comparison of the cumulative number of $T=0$ levels in ^{18}F and $T=1$ levels in ^{18}O to the integrated density, Eq. (4), defined by $N(E) = \sum_{J,\pi} \int_0^E dE_x \times \rho(E_x, J, \pi)$. The solid lines are computed using $\Delta(^{18}\text{F}) = 0$ MeV and $\Delta(^{18}\text{O}) = 2.25$ MeV. The dashed lines are exponential extrapolations of the experimental $N(E)$.

Secondly, there are a very large number of low-spin states that may contribute. Thus the fluctuating sum of their contributions to the cross section could be large, especially in cases where the fluctuations in Γ and $\langle H_c \rangle$ result in narrow levels or particularly strong mixing. Finally, for the $l = 1$ partial wave there should be contributions from the strong 1^- , $T = 1$ giant dipole resonance which is expected at about $E_x(^{18}\text{F}) = 20$ MeV.

VI. SPECTROSCOPY OF ^{18}F

This discussion emphasizes the isospin-mixed levels because the spin-parity restrictions on this particular isospin-forbidden reaction simplify the analysis and allow us to extract level parameters in the rather complex region of $10 \leq E_x(^{18}\text{F}) \leq 20$ MeV (see Sec. IV). The levels are characterized by mixed isospin, moderately narrow widths, natural parity, and $J \neq 0$. No such restrictions exist for our allowed transitions, and so we have not been able to identify individual levels except for a few at the lower energies. Having identified many isospin-mixed levels, we also wish to determine whether they are primarily $T = 1$ with $T = 0$ admixture (or vice versa), and the degree of mixing. If strongly mixed, we would like to determine the configurations involved, e.g. mirror cluster states.

Level Density and Statistical Fluctuations

The level density expected for $9 \leq E_x(^{18}\text{F}) \leq 20$ MeV is quite large, and we will estimate the value using the Fermi-gas model. The density is then²⁸

$$\rho(E_x, J, \pi) = 0.0295 a^{-1/4} u^{-5/4} \sigma^{-3} \exp[2(au)^{1/2}] \times (2J+1) \exp[-J(J+1)/2\sigma^2], \quad (4)$$

where $\sigma = g \langle m^2 \rangle t$; $g = (6/\pi^2)a$; $t = (u/a)^{1/2}$; $\langle m^2 \rangle = 0.24 A^{2/3}$; and $u = E_x - \Delta$. Marcazzan and Colli²⁸ give empirical values of a that fit the data for $E_x \leq 20$ MeV and $25 \leq A \leq 60$. Schier and Reber²⁹ use $a = A/8$ for ^{18}F . They also take the pairing energy, Δ , of ^{18}F as 0 and Δ of ^{18}O as ~ 3 MeV. We find $\Delta(^{18}\text{O}) = 2.25$ MeV gives a better match to the known number of low-lying levels of ^{18}O , see Fig. 20. The use of this statistically based formula may not be justified for so light a nucleus. However, Fig. 20 shows that it matches an exponential extrapolation of the cumulative number of $T = 0$ levels in ^{18}F and $T = 1$ levels in ^{18}O . (We have assumed that the first 30 levels have been identified in each nucleus). The number of $T = 1$ levels in ^{18}F should be equal to the number of levels in ^{18}O at $E_x(^{18}\text{O}) = E_x(^{18}\text{F}) - 1.04$ MeV. We will tentatively adopt the values calculated from Eq. (4) as being correct to at least a factor of 2.

Indirect support for the validity of Eq. (4) may come from an examination of our cross sections in terms of statistical fluctuations. However, the smallness of Γ_J/D_J for most of the ^{18}F data signals caution in drawing conclusions from fluctuation analyses. Earlier such analyses^{2,30} reported an average correlation width $\bar{\Gamma} \approx 200$ keV, but examination of our excitation function reveals that the low-energy structure is noticeably narrower than that at high energies. To display this variation with energy we adopt a peak-counting method of fluctuation analysis since this technique is less sensitive to finite range of data effects,³¹ is very simple to apply, and hopefully will indicate where fluctuation analysis is applicable.

Figure 21 shows the results of peak counting in intervals of 1-MeV bombarding energy. Plotted are the coherent widths, $\bar{\Gamma} = 0.55/k$ where k is the number of peaks per MeV.²⁸ The points are averages over all angles and we saw no systematic angle dependence. Because of the small intervals, the errors on individual points are too large to determine the functional form of $\bar{\Gamma}(E)$ but the trend of the data is obvious. Below $E_x \sim 12$ MeV the points probably reflect the spacing of prominent narrow levels, and at higher energies the local coherence width. The break occurs at the energy where Eq. (4) predicts that levels of $J = 1, 2, 3$ (which constitute $\sim 75\%$ of the levels at $E_x \sim 12$ MeV) all reach $\rho(J, \pi) = 6-8/\text{MeV}$, i.e., $\Gamma_J/D_J \sim 1$ and statistical effects should become more noticeable. The α_0 and α_2 results are similar, but $\bar{\Gamma}(\alpha_1)$ is usually smaller for $E_x > 14$ MeV. There are several pos-

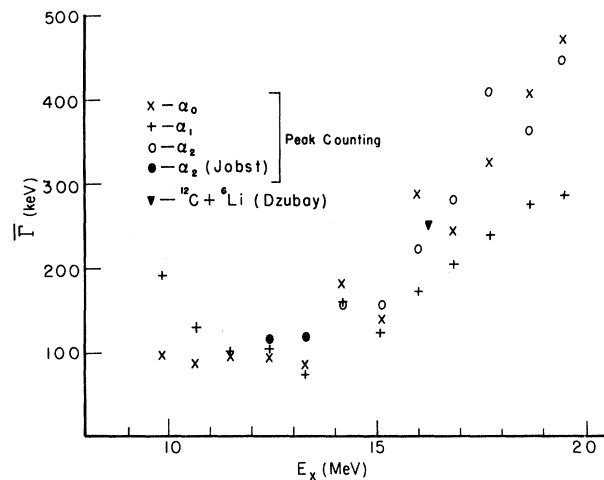


FIG. 21. Average coherence widths $\bar{\Gamma} = 0.55/k$ obtained by counting peaks in 1-MeV intervals where k is the number of peaks/MeV. The lower α_2 points are from the data of Ref. 2. The analysis of Dzubay, Ref. 30, is a standard autocorrelation analysis averaged over several final states.

sible explanations for the smaller $\bar{\Gamma}$ of the (d, α_1) channel. Bizzeti³² predicts that at the same excitation energy an isospin-forbidden reaction will show a smaller correlation width than an isospin-allowed reaction. Alternately, the (d, α_1) results of Fig. 21 for $E_x > 14$ MeV may reflect mainly the contribution of individual high-spin states since the cross sections have $(2l+1) = (2J+1)$ weighting factors³³ but low penetrability factors keep the width small.

The evidence described above for the validity of Eq. (4) is only suggestive. However, let us compare the number of isospin-mixed levels found in specific intervals with the predictions of Eq. (4). For this purpose we use intervals of excitation energy for each partial wave selected to correspond to the regions where we believe our data and analysis to be most reliable. For each l , the lower-energy limit comes from the Legendre polynomial analysis of the (d, α_0) data and corresponds to the energy where the coefficient a_{2l} or a_{2l-1} first becomes appreciable indicating that the (limiting) incoming l th partial wave channel has opened up. The upper limit is the energy where the $(l+1)$ partial wave is needed in the analysis of the isospin-forbidden reaction. In this manner we guarantee uniqueness of the $|S_l|$ in the region used. Table IV shows that the number of levels used to fit the (d, α_1) data falls somewhere between the number of predicted $T=0$ and $T=1$ levels. Although the number of levels is small, the results indicate that most of the 3^- and 5^- states in ^{18}F at these excitation energies have measurable isospin impurity independent of whether they are basically $T=0$ with a $T=1$ impurity or $T=1$ ($T=0$).

Analog States

The ^{18}O levels excited via $^{14}\text{C}(\alpha, \alpha)^{14}\text{C}$, except the 0^+ states, are the analogs to the $T=1$ ($T=0$) states of ^{18}F involved in the isospin-forbidden reaction. Such α elastic scattering populates only natural parity states of ^{18}O which have appreciable

α decay widths to the ground state of ^{14}C . The latter is the analog of the $^{14}\text{N}(2.31\text{-MeV}, T=1)$ state. Weinman and Silverstein²³ find such levels at $E_x(^{18}\text{O}) = 8.212$ and 8.282 MeV with $J^\pi = 2^+$ and 3^- , respectively, and then no structure for about 1 MeV. We also find 2^+ and 3^- levels near the corresponding energies, $E_x(^{18}\text{F}) = 9.32$ and 9.26 MeV. At these excitation energies, states in ^{18}O are well separated. Thus these ^{18}F levels are the analogs, and hence $T=1$ ($T=0$). Experimental difficulties at these low energies make it difficult to exclude the possibility of other weak states.

Morgan *et al.*³⁴ studied $^{14}\text{C}(\alpha, \alpha)^{14}\text{C}$ for $9 \leq E_x(^{18}\text{O}) \leq 19$ MeV and identify a number of levels below $E_x(^{18}\text{O}) = 13$ MeV. They assign spins and parities to 13 relatively strong but narrow resonances. However, their list is not complete as they also see several wide and/or weak resonances for which they make no assignments. In Table III we indicate which ^{18}F levels appear to be the analogs. The criteria used are similarities of spin and parity, energy, and approximate width.

Besides the analogs listed in Table III there are candidates for all the other levels Morgan *et al.* identify except for the 6^+ states at $E_x(^{18}\text{O}) = 11.69$ and 12.53 MeV. The 6^+ states definitely do not appear in our (d, α_1) data. The second 6^+ state is present¹⁰ in $^{14}\text{N}(\alpha, \alpha_1)^{14}\text{N}$ and we attribute the absences in our experiment to the small $l=6$ penetrabilities in the incoming deuteron channel. This interpretation is supported by the lack of measurable a_{11} and a_{12} in the Legendre polynomial expansion for (d, α_0) at or below the appropriate energy, $E_d < 7$ MeV. Since the $J^\pi = 6^+$ ($T=0$) level density is still small at these energies, the lower 6^+ ($T=1$) state may show very little mixing.

We next consider the region $9.7 \leq E_x(^{18}\text{F}) \leq 11.7$ MeV which has $l_{\max} = 3$ (except for the single 4^+ level at $E_d = 4.26$ MeV) and in which we have a good fit of the cross sections as well as the $|S_l|$'s. Thus the parameters in this region are the best we have. We find that 10 levels are needed to fit the unambiguous $l=3$ partial wave, whereas Morgan *et al.* list only two 3^- states in ^{18}O . However, other unidentified structure is present in their data. Equation (4) predicts approximately nine $T=0$ and three $T=1$ states for $l=3$. Our 10 levels are in remarkably good agreement if we assume that all of the predicted $T=0$ states have a measurable $T=1$ component. For this to be reasonable we need at least one more $T=1$ state below the two analogs which we associate with the large $|S_3|$ centered at $E_d = 3.4$ MeV. In the data of Morgan *et al.* there is a broad anomaly at $E_\alpha \sim 4.1$ MeV that appears to have a 3^- component. Perhaps our 3^- level at $E_d = 3.56$ MeV is the analog. We reiterate our confidence that the 3^- partial wave

TABLE IV. Comparison of the number of ^{18}F levels found in the isospin-forbidden analysis and the number expected from Eq. (4).

l	Energy range		Levels expected		Levels found (with T impurities)
	E_d (MeV)	E_x (MeV)	$T=0$	$T=1$	
1 ^a	1.8-5.4	9.2-12.3	17	4	7
2 ^a	1.8-5.4	9.2-12.3	18	6	18
3	1.8-5.4	9.2-12.3	14	4	13
4	3.2-5.6	10.4-12.6	7	2	2
5	4.5-8.0	11.6-14.8	10	3	8
6	7.0-11.5	13.7-17.8	13	4	5
7	11.0-14.0	17.3-19.8	8	3	3

^a Not the highest l needed in this region.

(Fig. 17) here requires 10 states in ^{18}F for its description. Thus unless this is an atypical clustering of 3^- levels, all (or nearly all) the 3^- states, both $T=0$ and $T=1$, are contributing to the forbidden reaction in this region.

If we examine the 1^- and 2^+ levels (where we expect about 12 $T=0$ and 5 $T=1$ levels in each case), we find 6 $l=1$ and 13 $l=2$ states. Both partial waves show much structure and we feel that 6 and 13 states are the minimum required to fit the data.

Two other isospin-forbidden reactions, $^{14}\text{N}(\alpha, \alpha_1)^{14}\text{N}$ and $^{12}\text{C}(^6\text{Li}, \alpha_1)^{14}\text{N}$ go through ^{18}F intermediate states and have the same exit channel as our data. Furthermore, they involve the same spin-parity combinations and so permit the same set of ^{18}F states.

The $^{12}\text{C}(^6\text{Li}, \alpha_1)^{14}\text{N}$ reaction is the least thoroughly studied.^{14, 30, 35} The low-energy data cover $15.25 \leq E_x(^{18}\text{F}) \leq 17.25$ MeV. The cross sections are small probably because of the large Coulomb barrier for ^6Li . Only partial waves $l=1, 2, 3$ appear important. The high-spin states of ^{18}F in this region apparently do not contribute because of the small penetrability for high partial waves in the incoming channel. Both at the low energies of Refs. 30 and 35 and for $E_{\text{Li}} > 9$ MeV [$E_x(^{18}\text{F}) \sim 20$ MeV] the yield of the forbidden reaction is $> 1\%$ of that for the allowed reactions.²⁷

Tollefsrud and Jolivet¹⁰ reported a partial-wave analysis for $^{14}\text{N}(\alpha, \alpha_1)^{14}\text{N}$ for $12.5 \leq E_x(^{18}\text{F}) \leq 14.5$ MeV. Their analysis predated our recent methods¹³ for choosing between ambiguous consistent sets of solutions, and so results for the low partial waves may not be meaningful. However, a number of resonances in high partial waves were clearly identified and probably are the same as those seen in the present experiment, Table III. The excitation energies and level widths do not match exactly, possibly because of uncertainties in the α energy loss in the target or the larger E_α steps, but more likely because the S matrix elements of the (α, α_1) data were not parametrized by coherent Breit-Wigner amplitudes to remove the interference effects in each partial wave. The only important discrepancy is for the 4^+ state at $E_x(^{18}\text{F}) = 12.5$ MeV which is well isolated in both experiments.¹⁰ Levels seen in (d, α_1) appear in (α, α_1) ; but some high-spin states, notably the 6^+ states at $E_x(^{18}\text{F}) = 13.405$ and 13.601 MeV, are not seen in (d, α_1) . As noted by Tollefsrud, generally $\Gamma_{\alpha_0} > \Gamma_{d_0}$ for high-spin states. Penetrabilities may explain this difference, or it may reflect an α cluster structure of ^{18}F . Chesterfield and Parker²⁶ also find that for high excitation energies $\sigma(\alpha, \alpha_1) > \sigma(d, \alpha_1)$ which is consistent with $\Gamma_{\alpha_0} > \Gamma_{d_0}$.

Isospin Mixing

Estimates of the isospin impurity, α^2 , have often been made using the ratio of the total cross sections for isospin-forbidden and -allowed reactions. The simplest formulation sets $\alpha^2 \approx R = \sigma(T=1)/\sigma(T=0)$. The underlying assumption is that the partial widths are proportional to the isospin impurities, i.e., if $\psi = \alpha|T=1\rangle + (1-\alpha^2)^{1/2}|T=0\rangle$ then $\sigma(T=1) \propto \Gamma_i \Gamma_0 \propto \alpha^2(1-\alpha^2)$ and $\sigma(T=0) \propto (1-\alpha^2)^2$. Because the contribution of the individual ^{18}F levels to our allowed data cannot be separated out, the above procedures are inapplicable for individual ^{18}F states. However, a meaningful average impurity, $\langle \alpha^2 \rangle$, can be calculated from a more sophisticated formulation,

$$\langle R_{\text{exp}} \rangle = \langle \alpha^2 \rangle R_0 f(\rho_T),$$

where now R_0 is the ratio expected from statistical theory in the absence of any isospin inhibition, and ρ_T is the density of states in ^{18}F of isospin T . Hauser-Feshbach calculations provide R_0 and for $E_x = 12$ MeV in ^{18}F give ~ 0.14 for the $d\alpha_i$ channels³⁶; ≈ 0.35 at $E_x = 14$ MeV for the $^{14}\text{N}(\alpha, \alpha_i)$ channels³⁷; and ≈ 0.18 at $E_x = 15$ MeV for the $^{12}\text{C}(^6\text{Li}, \alpha_i)$ channels.³⁰ For the same $E_x(^{18}\text{F})$ penetrabilities affect the incoming α channel less than the deuteron channel and much less than the ^6Li channel. At sufficiently high E_x all channels should give the same $R_0 = \frac{1}{5}$ which is the ratio of the number of independent amplitudes that contribute. The factor $f(\rho_T)$ arises because the forbidden cross section has contributions from $T=1$ components of $T=0$ levels as well as from primarily $T=1$ levels.²⁹ Tollefsrud³⁸ calculates for the present case that $f(\rho_T) \approx 2$. Thus, $\langle \alpha^2 \rangle \approx 5R/2$ and from Table II $\langle \alpha^2 \rangle$ varies between 3 and 10% for the intervals used. The presence of direct contributions to the allowed reactions would make this a lower limit, and the presence of wide levels in the compound nucleus means that the $\langle \alpha^2 \rangle$ measured is less than the actual mixing.

There is enough information from the (α, α_1) data of Ref. 10 and the present work to bypass the ratio method and calculate the partial widths of the $E_x = 12.50$ MeV (4^+) and narrow 12.70-MeV (5^-) states if we adopt the lower limit of $\Gamma \geq \sum \Gamma_i$ and assume that the only channels open are d_0 , α_0 , and α_1 . Penetrabilities indicate that the latter assumption might be a good approximation for these relatively high-spin states. Then using the level parameters from Table III and Ref. 10 and noting that the Legendre polynomial expansion for (d, α_0) has small a_8 and a_{10} at the appropriate energies (see Fig. 15) we conclude that Γ_{α_1} is 0.96Γ and 0.98Γ for the 4^+ and 5^- levels, respectively. The dominance of the α_1 decay confirms that these are

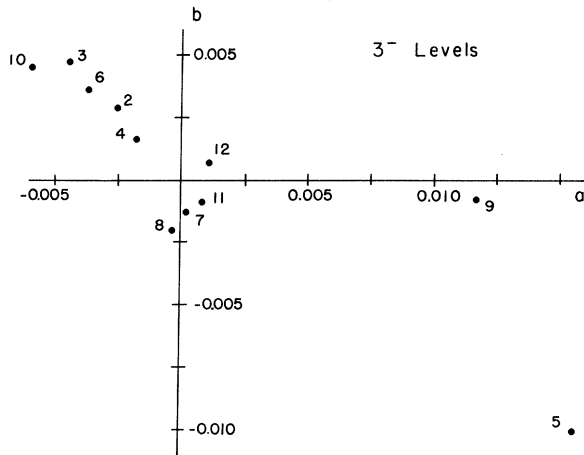


FIG. 22. Plots of the complex amplitudes of the first twelve 3^- levels of Table III.

$T=1(T=0)$ analogs. If we assume that $\alpha^2/(1-\alpha^2) = \Gamma_{T=0}/\Gamma_{T=1}$, then we need small isospin mixing, ~ 4 and 2% $T=0$ intensities, respectively, for the 4^+ and 5^- levels, even though the cross sections are among the largest observed in either isospin-forbidden reaction. The assumptions made undoubtedly cause Γ_{α_1} to be overestimated. While apparently we see the same two ^{18}F levels via the (d, α_1) and the (α, α_1) channels, the possibility remains that each level could be a T doublet with one member of each pair having a large Γ_{α_0} and a small Γ_{d_0} and vice versa.

In general we do not have enough information about the partial widths to estimate the isospin impurities of individual levels in the manner described above. More detailed information about the strength of the isospin mixing and possibly about which states are mixed should be available in the Breit-Wigner amplitudes used to fit the data. In the simple case where only two levels mix the normalized wave functions would be

$$\begin{aligned}\psi_a &= \alpha |0\rangle + \beta |1\rangle, \\ \psi_b &= -\beta |0\rangle + \alpha |1\rangle.\end{aligned}\quad (5)$$

Then the amplitudes for an isospin-forbidden reaction through the two states of the isospin doublet are $A_a \propto \alpha\beta$ and $A_b \propto -\alpha\beta$, i.e., the amplitudes are equal and of opposite sign. This would be one signature of mirror cluster states. Figures 22 and 23 show the plots of the complex amplitudes for the best-determined 3^- and 5^- levels. The figures show that there is a tendency for neighboring states to be near a line through the origin, but the simple relationship described above is not in general a good description. The first two 5^- levels are perhaps closest to the simple case. There is a

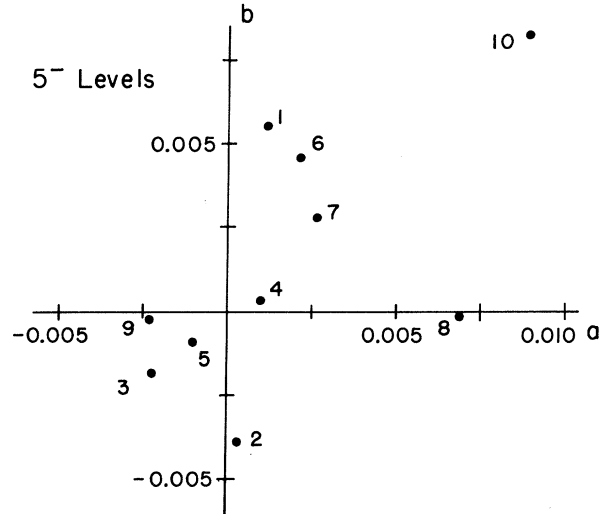


FIG. 23. Plots of the complex amplitudes of the first ten 5^- levels of Table III.

greater tendency for several levels to add up to approximately zero total amplitude, for example the 5^- levels 2-6. Friedman³⁹ finds that correcting for penetrabilities improves the sum rule. Apparently mirror cluster doublets are not common, but fragments of a mirror configuration may spread over a number of nearby states. Analysis in terms of fragmented bridge states seems promising.³⁹

VII. SUMMARY

The allowed transitions studied are predominantly compound nuclear and the isospin-forbidden transition appears exclusively so. The average isospin impurity in ^{18}F for $10 \leq E_x \leq 20$ MeV is 3-10% and estimates for two individual levels are also small. Of the many isospin-mixed levels found in the forbidden reaction some can be identified as analogs of $T=1$ states in ^{18}O . However, there are enough resonances seen to indicate that a large proportion of the primarily $T=0$ levels also contribute. The level densities appear to be consistent with predictions of the Fermi-gas model and the average coherence width is found to increase rapidly with energy.

ACKNOWLEDGMENTS

I would like to thank Professor H. T. Richards for his help and encouragement, and Professor C. H. Blanchard, Professor W. A. Friedman, and Professor K. W. McVoy for several helpful discussions. I also thank Dr. H. V. Smith, Dr. R. J. Nickles, Dr. P. B. Tollefsrud, Dr. M. J. Wozniak, G. Klody, S. Wilson, and the others who helped with various parts of the work.

- *Work supported in part by the U. S. Atomic Energy Commission.
- †Present address: Department of Physics, University of Notre Dame, Notre Dame, Indiana 46556.
- ¹F. Ajzenberg-Selove, Nucl. Phys. A190, 1 (1972).
- ²J. Jobst, Phys. Rev. 168, 1156 (1968).
- ³H. Cords, G. U. Din, and B. A. Robson, Nucl. Phys. A134, 561 (1969).
- ⁴J. V. Noble, Phys. Rev. 173, 1034 (1968).
- ⁵J. V. Noble, Phys. Rev. Lett. 22, 473 (1969).
- ⁶D. H. Wilkinson, Phil. Mag. 1, 379 (1956).
- ⁷A. M. Lane and R. G. Thomas, Rev. Mod. Phys. 30, 257 (1958).
- ⁸P. L. Jolivette and H. T. Richards, Phys. Rev. 188, 1660 (1969).
- ⁹J. Jobst, S. Messelt, and H. T. Richards, Phys. Rev. 178, 1663 (1969).
- ¹⁰P. B. Tollefsrud and P. L. Jolivette, Phys. Rev. C 1, 398 (1970).
- ¹¹P. L. Jolivette, Ph.D. thesis, University of Wisconsin, 1970 (unpublished). Available through University Microfilms, Inc., Ann Arbor, Michigan. The complete cross-section data for α_0 and α_1 are available in tabular form. See NAPS document 02185 for 86 pages of material on α_0 and NAPS document 02186 for 89 pages on α_1 . Order from ASIS/NAPS, c/o Microfiche Publications, 305 East 46th Street, New York, N.Y. 10017. Remit in advance for each NAPS accession number \$1.50 for microfiche or \$13.40 for a photocopy of 02185 and \$13.85 for a photocopy of 02186.
- ¹²O. Dietzsch, R. A. Douglas, E. Farrelly Pessoa, V. Gomes Porto, E. W. Hamburger, T. Polga, and O. Sala, Nucl. Phys. A114, 330 (1968).
- ¹³P. L. Jolivette, Phys. Rev. Lett. 26, 1383 (1971).
- ¹⁴T. G. Dzubay, Ph.D. thesis, University of Minnesota, 1966 (unpublished). Available through University Microfilms, Inc., Ann Arbor, Michigan.
- ¹⁵T. Yanabu, S. Yamashita, T. Nakamura, K. Takumatsu, A. Masaike, S. Kakigi, D. C. Nguyen, and K. Takimoto, J. Phys. Soc. Jap. 18, 747 (1963); 16, 2594 (1961); T. Yanabu, *ibid.* 16, 2118 (1961).
- ¹⁶T. Honda, H. Horie, Y. Kudo, and H. Ui, Progr. Theor. Phys. 31, 424 (1964).
- ¹⁷T. Ericson, Ann. Phys. (N.Y.) 23, 390 (1963).
- ¹⁸J. Jänecke, T. F. Yang, W. S. Gray, and R. M. Polichar, Phys. Rev. C 3, 79 (1971).
- ¹⁹J. Jänecke, T. F. Yang, R. M. Polichar, and W. S. Gray, Phys. Rev. 175, 1301 (1968).
- ²⁰R. J. Drachman, Phys. Rev. Lett. 17, 1017 (1966).
- ²¹F. A. Griffy, Phys. Lett. 21, 693 (1966).
- ²²W. M. MacDonald, Phys. Rev. 101, 271 (1956).
- ²³J. A. Weinman and E. A. Silverstein, Phys. Rev. 111, 277 (1958).
- ²⁴F. C. Barker, Nucl. Phys. 83, 418 (1966).
- ²⁵W. J. Braithwaite, J. E. Bussoletti, F. E. Cecil, and G. T. Garvey, Phys. Rev. Lett. 29, 376 (1972).
- ²⁶C. M. Chesterfield and P. D. Parker, Bull. Am. Phys. Soc. 15, 1654 (1970).
- ²⁷J. P. Sokol, private communication.
- ²⁸M. G. Braga Marcazzan and L. Milazzo Colli, in *Progress in Nuclear Physics*, edited by D. M. Brink and J. H. Mulvey (Pergamon, New York, 1970).
- ²⁹W. A. Schier and J. D. Reber, Phys. Rev. 181, 1371 (1969).
- ³⁰T. G. Dzubay, Phys. Rev. 158, 977 (1967).
- ³¹A. Van der Woude, Nucl. Phys. 80, 14 (1966).
- ³²P. G. Bizzeti, Phys. Lett. 13, 334 (1964).
- ³³When $\Gamma_{J\pi}/D_{J\pi}$ is large and fluctuations dominate the cross section, our partial-wave decomposition of the isospin-forbidden reaction is still valid. However, the expansion of a given partial wave in terms of a unique set of Breit-Wigner resonances becomes more difficult. For the high partial waves which have a lower level density we feel more confident that we have extracted the correct set of overlapping levels.
- ³⁴G. L. Morgan, D. R. Tilley, G. E. Mitchell, R. A. Hilko, and N. B. Roberson, Nucl. Phys. A148, 480 (1970).
- ³⁵R. R. Carlson and D. W. Heikkinen, Phys. Lett. 17, 305 (1965).
- ³⁶Y. Hashimoto and W. P. Alford, Phys. Rev. 116, 981 (1959).
- ³⁷C. M. Chesterfield, Ph.D. thesis, University of Melbourne (unpublished).
- ³⁸P. B. Tollefsrud, Ph.D. thesis, University of Wisconsin (1969). Available through University Microfilms, Inc., Ann Arbor, Michigan.
- ³⁹W. A. Friedman, Bull. Am. Phys. Soc. 17, 904 (1972); Phys. Rev. Lett. 30, 394 (1973).